SLC25A23 augments mitochondrial Ca^{2+} uptake, interacts with MCU, and induces oxidative stress–mediated cell death

Nicholas E. Hoffman[a,b], Harish C. Chandramoorthy[a,b], Santhanam Shanmughapriya[a,b], Xueqian Q. Zhang[b], Sandhya Vallem[b], Patrick J. Doonan[a,b,*], Karthik Malliankaraman[a,b,†], Shuchi Guo[b], Sudarsan Rajan[a,b], John W. Elrod[b], Walter J. Koch[b], Joseph Y. Cheung[b], and Muniswamy Madesh[a,b]

[a]Department of Biochemistry and [b]Center for Translational Medicine, Temple University, Philadelphia, PA 19140

ABSTRACT **Emerging findings suggest that two lineages of mitochondrial Ca^{2+} uptake participate during active and resting states: 1) the major eukaryotic membrane potential–dependent mitochondrial Ca^{2+} uniporter and 2) the evolutionarily conserved exchangers and solute carriers, which are also involved in ion transport. Although the influx of Ca^{2+} across the inner mitochondrial membrane maintains metabolic functions and cell death signal transduction, the mechanisms that regulate mitochondrial Ca^{2+} accumulation are unclear. Solute carriers—solute carrier 25A23 (SLC25A23), SLC25A24, and SLC25A25—represent a family of EF-hand–containing mitochondrial proteins that transport Mg-ATP/Pi across the inner membrane. RNA interference–mediated knockdown of SLC25A23 but not SLC25A24 and SLC25A25 decreases mitochondrial Ca^{2+} uptake and reduces cytosolic Ca^{2+} clearance after histamine stimulation. Ectopic expression of SLC25A23 EF-hand–domain mutants exhibits a dominant-negative phenotype of reduced mitochondrial Ca^{2+} uptake. In addition, SLC25A23 interacts with mitochondrial Ca^{2+} uniporter (MCU; CCDC109A) and MICU1 (CBARA1) while also increasing I_{MCU}. In addition, SLC25A23 knockdown lowers basal mROS accumulation, attenuates oxidant-induced ATP decline, and reduces cell death. Further, reconstitution with short hairpin RNA–insensitive SLC25A23 cDNA restores mitochondrial Ca^{2+} uptake and superoxide production. These findings indicate that SLC25A23 plays an important role in mitochondrial matrix Ca^{2+} influx.**

Monitoring Editor
Thomas D. Fox
Cornell University

Received: Aug 29, 2013
Revised: Dec 31, 2013
Accepted: Jan 7, 2014

INTRODUCTION

The Ca^{2+} signals in the mitochondria regulate key cellular functions such as energy production and cell death. The transport of Ca^{2+} across the inner mitochondrial membrane is an essential signaling pathway for cellular metabolic functions. Although basal cytosolic Ca^{2+} levels are maintained at ~100 nM, upon agonist-induced cytosolic Ca^{2+} increase, Ca^{2+} is sequestered by Ca^{2+}-binding proteins, the endoplasmic reticulum (ER), and mitochondria, which accumulate large amounts of Ca^{2+} (Nicholls, 2005; Rizzuto *et al.*, 2012). Although the mitochondrial Ca^{2+} uniporter (MCU) has low affinity, mitochondrial Ca^{2+} overload can occur during times of stress because mitochondria are in close proximity to the ER (Rizzuto *et al.*, 1998, 2004). In addition to the MCU (Baughman *et al.*, 2011; De Stefani *et al.*, 2011), its regulators, mitochondrial Ca^{2+} uptake1 (MICU1) and mitochondrial Ca^{2+} uniporter regulator 1 (MCUR1), were also identified (Perocchi *et al.*, 2010; Mallilankaraman *et al.*, 2012a,b; Hoffman *et al.*, 2013). The recent discovery of molecular MCU constituents raises the possibility of examining Ca^{2+} uptake relationships between different mitochondrial protein systems. Here we examine the relationship between MCU and a distinct family of solute carriers (SLC family).

Solute carriers in the mitochondria can be divided into two major groups: aspartate/glutamate carriers (Palmieri *et al.*, 2001) and ATP-magnesium carriers (Satrustegui *et al.*, 2007b), of which solute

This article was published online ahead of print in MBoC in Press (http://www.molbiolcell.org/cgi/doi/10.1091/mbc.E13-08-0502) on January 15, 2014.

Present addresses: *Department of Pathobiology and †Department of Physiology, University of Pennsylvania, Philadelphia, PA 19140.

Address correspondence to: Muniswamy Madesh (madeshm@temple.edu).

Abbreviations used: $\Delta\Psi_m$, mitochondrial membrane potential; MCU, mitochondrial Ca^{2+} uniporter; MCUR1, mitochondrial Ca^{2+} uniporter regulator 1; MICU1, mitochondrial Ca^{2+} uptake 1; SLC25A23, solute carrier 25A23.

carrier 25A23 (SLC25A23), SLC25A24, and SLC25A25 are paralogues. SLC25A23 and SLC25A24 transport adenine nucleotides in response to Ca^{2+} (Aprille, 1988; Fiermonte *et al.*, 2004; Tewari *et al.*, 2012; Traba *et al.*, 2012; Amigo *et al.*, 2013), but the functional interplay with mitochondrial Ca^{2+} uptake has not yet been rigorously characterized. However, it has been reported that the deletion of SLC25A23 diminishes oxidative phosphorylation (Amigo *et al.*, 2013). Further, SLC25A23, SLC25A24, and SLC25A25 contain functional EF hands (Bassi *et al.*, 2005), which makes their Mg/ATP-Pi carrier function Ca^{2+} sensitive, similar to other Ca^{2+}-activated channels and carriers. Mitochondrial solute carriers are widespread in eukaryotes and well conserved (Carafoli and Lehninger, 1971; Uribe *et al.*, 1992; Palmieri, 2004, 2013). For example, Sal1 is a yeast homologue to SLC25A23 that also contains EF-hand domains (Kucejova *et al.*, 2008). The double inactivation of yeast Sal1 and ATP/ADP translocase (aac2) leads to abnormal mitochondrial DNA. The activation of these solute carriers occurs on the exterior of the inner mitochondrial membrane (Haynes *et al.*, 1986; Nosek *et al.*, 1990; Palmieri *et al.*, 2001), and activators include Ca^{2+}, adenosine 3′5′-cyclical monophosphate, protein kinases, and inositol polyphosphates (Dransfield and Aprille, 1993). Members of the SLC25 family have been identified as the cause of Stanley syndrome (SLC25A20) and Amish microcephaly (SLC20A19), suggesting the functional importance of SCaMCs (Palmieri, 2004; Molinari *et al.*, 2005, 2009). Similar to Sal1, SLC25A24 is involved in regulating the ADP/ATP ratio in mitochondrial matrix (Traba *et al.*, 2012). However, a recent study using the SLC25A25-knockout mouse showed only moderate effects on metabolism (Anunciado-Koza *et al.*, 2011).

In our search for the molecular identity of the MCU, the group SLC25A23, SLC25A24, and SLC25A25 emerged as being of interest (Mallilankaraman *et al.*, 2012a). They were selected for study because they are predicted to form multitransmembrane domains, sense Ca^{2+} with functional Ca^{2+}-binding EF-hand motifs, and localize to the mitochondrial inner membrane (del Arco and Satrustegui, 1998, 2004; Iijima *et al.*, 2001). SLC25A23 is highly expressed in brain, heart, skeletal muscle, liver, and small intestine (Bassi *et al.*, 2005), and although SLC25A23 has been characterized as a Ca^{2+}-activated ATP-Mg/Pi carrier, the functional interplay and feedback provided by SLC25A23 activity on mitochondrial Ca^{2+} uptake remain unknown.

The purpose of this work is to investigate how this family of solute carriers regulates mitochondrial Ca^{2+} uptake, bioenergetics, and cell survival. Here we report that knockdown of SLC25A23 reduces mitochondrial Ca^{2+} uptake while interacting with MCU and MICU1, without altering mitochondrial efflux. The EF-hand domains of SLC25A23 are necessary for its function and thus participate in mitochondrial matrix Ca^{2+} accumulation and stress-induced cell death.

RESULTS

Silencing of SLC25A23 modulates mitochondrial Ca^{2+} uptake

To explore the role of SLC25 isoforms, we stably knocked down SLC25A23, SLC25A24, and SLC25A25 using lentiviral short hairpin RNA (shRNA; Mallilankaraman *et al.*, 2012a). We subjected puromycin-resistant, stably expressing lentiviral shRNA HeLa cell clones to quantitative real-time (qRT) PCR to assess SLC25 mRNA levels (Figure 1, A–C). We next examined whether the SLC25A23 #864 shRNA was exclusively on-target, by assessing mRNA levels of SLC25A23, SLC25A24, and SLC25A25 in the SLC25A23 #864 shRNA HeLa clone. As expected, SLC25A23 but not SLC25A24 or SLC25A25 mRNA was knocked down (Supplemental Figure S1), confirming the specificity of the #864 shRNA. HeLa cell maximal knockdown clones #864, #594, and #739 for SLC25A23, SLC25A24, and SLC25A25, respectively, were assayed using confocal microscopy for cytosolic Ca^{2+} (Fluo-4) and mitochondrial Ca^{2+} (Rhod-2 AM) dynamics after stimulation with the G-protein–coupled receptor (GPCR) agonist histamine (100 µM; Madesh *et al.*, 2005; Hawkins *et al.*, 2010a,b; Davidson and Duchen, 2012; Mallilankaraman *et al.*, 2012a,b). SLC25A23 knockdown (KD) but not SLC25A24 KD or SLC25A25 KD exhibited diminished mitochondrial Ca^{2+} uptake (Figure 1, D–F, bottom left). To complement the rhod-2 AM results, we transfected HeLa SLC25A23 KD, SLC25A24 KD, and SLC25A25 KD clones with the genetic mitochondrial Ca^{2+} reporter GCaMP2-mt and assayed after histamine (100 µM) stimulation. GCaMP2-mt fluorescence corroborated that SLC25A23 KD reduces mitochondrial Ca^{2+} uptake, whereas SLC25A24 KD and SLC25A25 KD are unaltered (Figure 1, G–J). Having observed a reduction of mitochondrial Ca^{2+} uptake by SLC25A23 KD but not SLC25A24 KD or SLC25A25 KD, we assessed cytosolic Ca^{2+} clearance after histamine stimulation. Cytosolic Ca^{2+} measured by Fluo-4 was examined in an extended time interval to evaluate whether decreased mitochondrial Ca^{2+} uptake in SLC25A23 KD reciprocally sustained cytosolic $[Ca^{2+}]$ (Quintana *et al.*, 2007). HeLa SLC25A23 KD and Neg shRNA cells were challenged with histamine, and fluorescence was recorded for 1000 s (Figure 1K). Quantitation of the cytosolic Ca^{2+} fluorescence area under the curve demonstrated marked deceleration of cytosolic Ca^{2+} clearance (Figure 1L).

SLC25A23 KD decreases mitochondrial Ca^{2+} uptake without altering efflux rate

To demonstrate that indeed SLC25A23 KD reduced mitochondrial Ca^{2+} uptake, we suspended permeabilized HeLa cells in intracellular matrix (ICM) buffer containing succinate to energize the mitochondria, thapsigargin to inhibit ER Ca^{2+} uptake via sarco/endoplasmic reticulum Ca^{2+} ATPase (SERCA), and added Fura-2FF to monitor extramitochondrial changes. We then pulsed cells with 10 µM Ca^{2+} to measure the mitochondrial Ca^{2+} uptake rate. Although the influx pathway is described by the rapid Ca^{2+} uptake channel MCU, Ca^{2+} efflux is mediated by the Na^{+}/Ca^{2+} exchanger, with a distinct, relatively slow kinetic rate. Ca^{2+} efflux was measured by blocking the major Ca^{2+} uptake channel, the mitochondrial uniporter, with Ru360 (Zhou *et al.*, 1998; Hajnoczky *et al.*, 2006), followed by blockage of the mitochondrial Na^{+}/Ca^{2+} exchanger with CGP37157 (Cox *et al.*, 1993; Palty *et al.*, 2010; Wei *et al.*, 2011). Finally, uncoupler carbonyl cyanide *m*-chlorophenyl hydrazone (CCCP) was added to trigger release of all mitochondria-stored Ca^{2+}, thus validating that equal amounts of total Ca^{2+} were pulsed. SLC25A23 KD only altered mitochondrial Ca^{2+} influx (Figure 2, A–C), whereas efflux rate and total mitochondrial $[Ca^{2+}]$ were unchanged (Figure 2, A, D, and E). Although statistically insignificant, a trend seemed to exist in the SLC25A23 KD total Ca^{2+} in which total SLC25A23 KD Ca^{2+} was reduced from Neg shRNA, presumably due to reduced influx rate. Knockdown of SLC25A24 and SLC25A25 did not alter influx rate, efflux rate, and total mitochondrial $[Ca^{2+}]$ (Supplemental Figure S2). The intact and permeabilized cell data indicate a SLC25A23 role in mitochondrial Ca^{2+} uptake.

SLC25A23 EF hands are necessary for mitochondrial Ca^{2+} uptake

SLC25A23 is predicted to be a multitransmembrane, mitochondrial-resident protein with three EF-hand motifs. After examining the EF-hand consensus sequence, we determined that only two of the three EF-hand motifs contain functional Ca^{2+}-binding sites. To investigate the role of Ca^{2+}-sensing properties of SLC25A23, we overexpressed GFP-tagged mutants of the two EF hands (EF1 D22A/E33K and EF2 D90A/E101K) in SLC25A23 KD cells

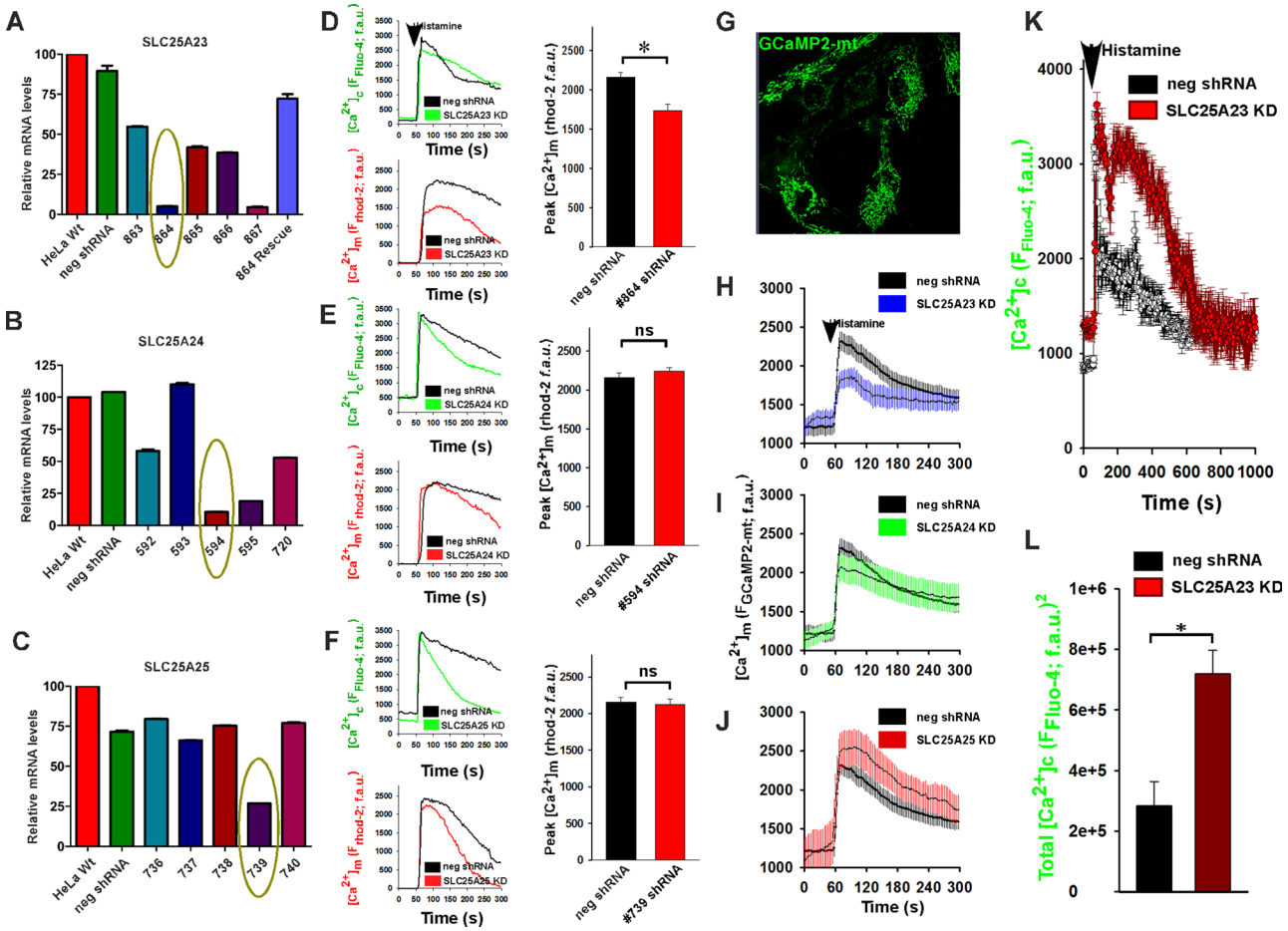

FIGURE 1: RNA interference–mediated silencing of SLC25A23, SLC25A24, and SLC25A25 reveals that SLC25A23 reduces mitochondrial Ca^{2+} uptake. (A) qRT-PCR results of SLC25A23 KD, (B) SLC25A24 KD, and (C) SLC25A25 KD clones. SLC25A23 KD clones #864 and #867 show reduced mRNA levels by 95 and 95.2%, respectively. (D) HeLa cells were stimulated with 100 μM histamine at 50 s. SLC25A23 clone 864 shRNA cytosolic Ca^{2+} trace (top left), mitochondrial Ca^{2+} trace (bottom left), and quantitation of mitochondrial rhod-2 fluorescence (right). (E) SLC25A24 clone 594 shRNA cytosolic Ca^{2+} trace (top left), mitochondrial Ca^{2+} trace (bottom left), and quantitation of mitochondrial Ca^{2+} uptake (right). (F) SLC25A25 clone 739 shRNA cytosolic Ca^{2+} trace (top left), mitochondrial Ca^{2+} trace (bottom left), and quantitation of mitochondrial Ca^{2+} uptake (right). (G) Representative image of transiently transfected HeLa cells expressing mitochondria-targeted Ca^{2+} indicator GCaMP2. (H) GCaMP2-mt HeLa cells were stimulated with 100 μM histamine at 60 s. SLC25A23 clone 864 mitochondrial Ca^{2+} trace (GCaMP2; scale 0–4096 f.a.u.). (I) SLC25A24 KD mitochondrial Ca^{2+} trace. (J) SLC25A25 KD mitochondrial Ca^{2+} trace. (K) SLC25A23 KD and Neg shRNA HeLa cells cytosolic Ca^{2+} clearance trace (Fluo-4; scale 0–4096 f.a.u.). (L) Quantitation of cytosolic Ca^{2+} clearance as area under the curve. Data are mean ± SEM (n = 3–5). *p < 0.05 compared with Neg shRNA.

(Figure 3A). Expression and mitochondrial localization were verified with mitochondrial membrane potential ($\Delta\Psi_m$) indicator tetramethylrhodamine ethyl ester (TMRE; Figure 3B). After verifying transient expression of SLC25A23 EF-hand mutants, we loaded HeLa cells with Rhod-2 AM and stimulated them with histamine. The EF-hand mutants exhibited a reduction of mitochondrial Ca^{2+} uptake (Figure 3, C and D). These data suggest that the EF hands are essential for SLC25A23 Ca^{2+} sensing and that SLC25A23 EF hands function to increase mitochondrial Ca^{2+} uptake.

SLC25A23 interacts with mitochondrial Ca^{2+} uniporter complex components MCU and MICU1

To determine the mechanism by which SLC25A23 modulates mitochondrial Ca^{2+} uptake, we asked whether SLC25A23 interacts with MCU or MICU1. Flag-tagged SLC25A23 was transfected into COS7 cells stably expressing GFP-tagged, full-length MCU or hemagglutinin (HA)-tagged full-length MICU1. The cell lysates from transfected cells were subjected to immunoprecipitation and Western blot analysis. Immunoprecipitation of GFP-tagged MCU pulled down SLC25A23 (Figure 4A) with MCU/MICU1 known interaction serving as a positive control. Correspondingly, HA-tagged MICU1 pulled down SLC25A23 (Figure 4B). The results of the coimmunoprecipitation demonstrate that SLC25A23 interacts with MCU and MICU1, two proteins believed to be of critical importance to mitochondrial Ca^{2+} influx.

Given that SLC25A23 interacts with MCU, we next sought to determine whether the knockdown of SLC25A23 modulates MCU activity (I_{MCU}). To measure I_{MCU}, we performed mitoplast patch clamping. In the patch clamp of whole-mitoplast configuration, the addition of 5 mM Ca^{2+} to the bath triggered an inwardly rectifying Ca^{2+} current, which was reduced in SLC25A23 KD mitoplasts in the nominal phosphate buffer condition (Figure 4, C and E). Because SLC25A23 was previously described as a Mg-ATP/Pi carrier (Fiermonte *et al.*, 2004), we measured the I_{MCU} in Neg shRNA and

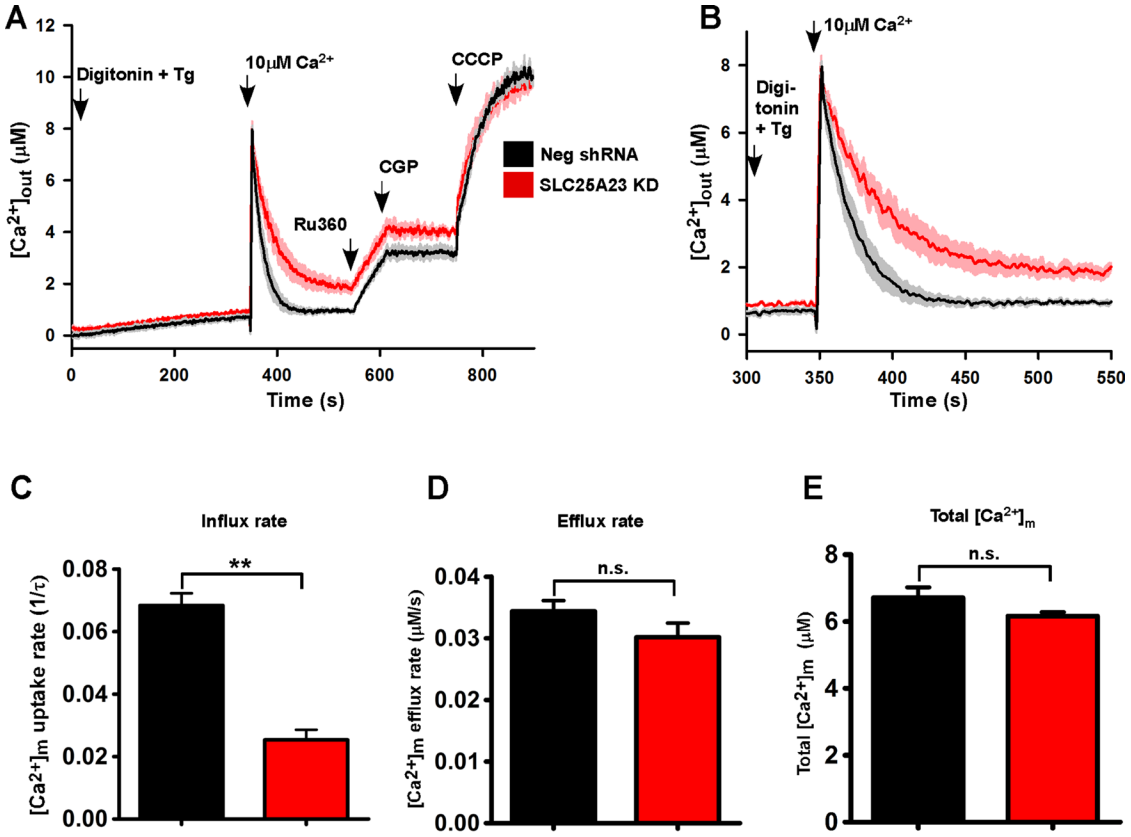

FIGURE 2: Knockdown of SLC25A23 reduces mitochondrial Ca^{2+} uptake rate. (A) Average traces with mean data point for each time point plotted with SE of permeabilized (40 μg/ml digitonin) HeLa cells loaded with the ratiometric Ca^{2+} indicator Fura2-FF and pulsed with 10 μM Ca^{2+} at 350 s to measure mitochondrial Ca^{2+} uptake, followed by addition of 1 mM RU360 at 550 s, 10 μM CGP37157 at 610 s and 2 μM uncoupler CCCP at 750 s. SLC25A23 KD showed reduced extra mitochondrial Ca^{2+} clearance. (B) Zoom of Ca^{2+} uptake from A (between 300 and 550 s). (C) Quantitation of Ca^{2+} influx rate. (D) Quantitation of Ca^{2+} efflux rate after addition of Ru360. (E) Quantitation of CCCP-induced Ca^{2+} release shows no significant difference in total Ca^{2+}. Data are mean ± SEM ($n = 3$). $^{**}p < 0.01$ compared with Neg shRNA; n.s., not significant.

SLC25A23 KD mitoplasts supplemented with 300 μM phosphate (Zoccarato and Nicholls, 1982; Figure 4, D and E). The I_{MCU} was increased by the presence of phosphate in Neg shRNA but not in SLC25A23 KD mitoplasts (Figure 4, C–E). This result suggests that the Mg-ATP/Pi carrier function of SLC25A23 enhances I_{MCU} activity.

Mitochondrial Ca^{2+} uptake reduction by SLC25A23 KD preserves $\Delta\Psi_m$

Because mitochondria Ca^{2+} uptake relies on $\Delta\Psi_m$ as a driving force, we asked whether the reduced mitochondrial Ca^{2+} uptake exhibited by SLC25A23 knockdown was due to a difference in basal driving force, $\Delta\Psi_m$. HeLa cells with maximal knockdown (clone 864) and moderate knockdown (clone 863) and a SLC25A23 rescue construct (Figure 1A and Supplemental Figure S3) showed neither $\Delta\Psi_m$ nor basal morphological phenotype changes when compared with a Neg shRNA HeLa cell clone, using two different $\Delta\Psi_m$ indicators, TMRE and rhodamine 123 (Figure 5, A and B). These data show that SLC25A23 knockdown does not alter basal $\Delta\Psi_m$.

We next examined active-state mitochondrial Ca^{2+} handling and $\Delta\Psi_m$ simultaneously using a permeabilized cell system loaded with cytosolic Ca^{2+} indicator Fura-2FF and $\Delta\Psi_m$ indicator JC-1 (Madesh and Hajnoczky, 2001; Madesh *et al.*, 2002, 2009; Roy *et al.*, 2009; Mallilankaraman *et al.*, 2012a,b). JC-1 is preferred to $DiOC_6(3)$ and rhodamine 123 in $\Delta\Psi_m$ studies when $\Delta\Psi_m$ may collapse (Salvioli *et al.*, 1997), which occurs when excessive Ca^{2+} is taken into the mitochondria. We found that the extramitochondrial delivery of Ca^{2+} pulses promoted a larger decay of $\Delta\Psi_m$ in control shRNA HeLa cells than with SLC25A23 #864 knockdown HeLa cells (Figure 5, C and D). Intermediate knockdown of SLC25A23 (#863) partially preserved $\Delta\Psi_m$ (Figure 5, C, bottom left, and D). We next verified SLC25A23's role by reexpressing #864 shRNA–insensitive SLC25A23 cDNA. We were able to restore Ca^{2+} flux and associated $\Delta\Psi_m$ (Figure 3, C, bottom right, and D). These results suggest that SLCA25A23 participates in mitochondrial Ca^{2+}-uptake regulation.

SLC25A23 increases basal reactive oxygen species and decreases antioxidant levels

Because SLC25A23 is involved in Ca^{2+}-activated adenine nucleotide transport, we examined mitochondrial DNA (mtDNA) copy number. Depletion of mitochondrial DNA copy number results in disassembly of electron transport chain components and thus drives reactive oxygen species (ROS) overproduction and mitochondrial malfunction (Hom *et al.*, 2010). We found that KD of SLC25A23 did not alter mtDNA copy number in HeLa cells when compared with either negative or partial KD (#863) shRNA clones (Figure 6, A and B), supporting our finding of no gross mitochondrial abnormalities. In complement, we also studied the mitochondrial oxygen consumption rate (OCR) and NAD(P)H levels. Silencing of SLC25A23 in HeLa cells did not significantly alter mitochondrial OCR and NAD(P)H content (Supplemental Figure S4). We next investigated whether

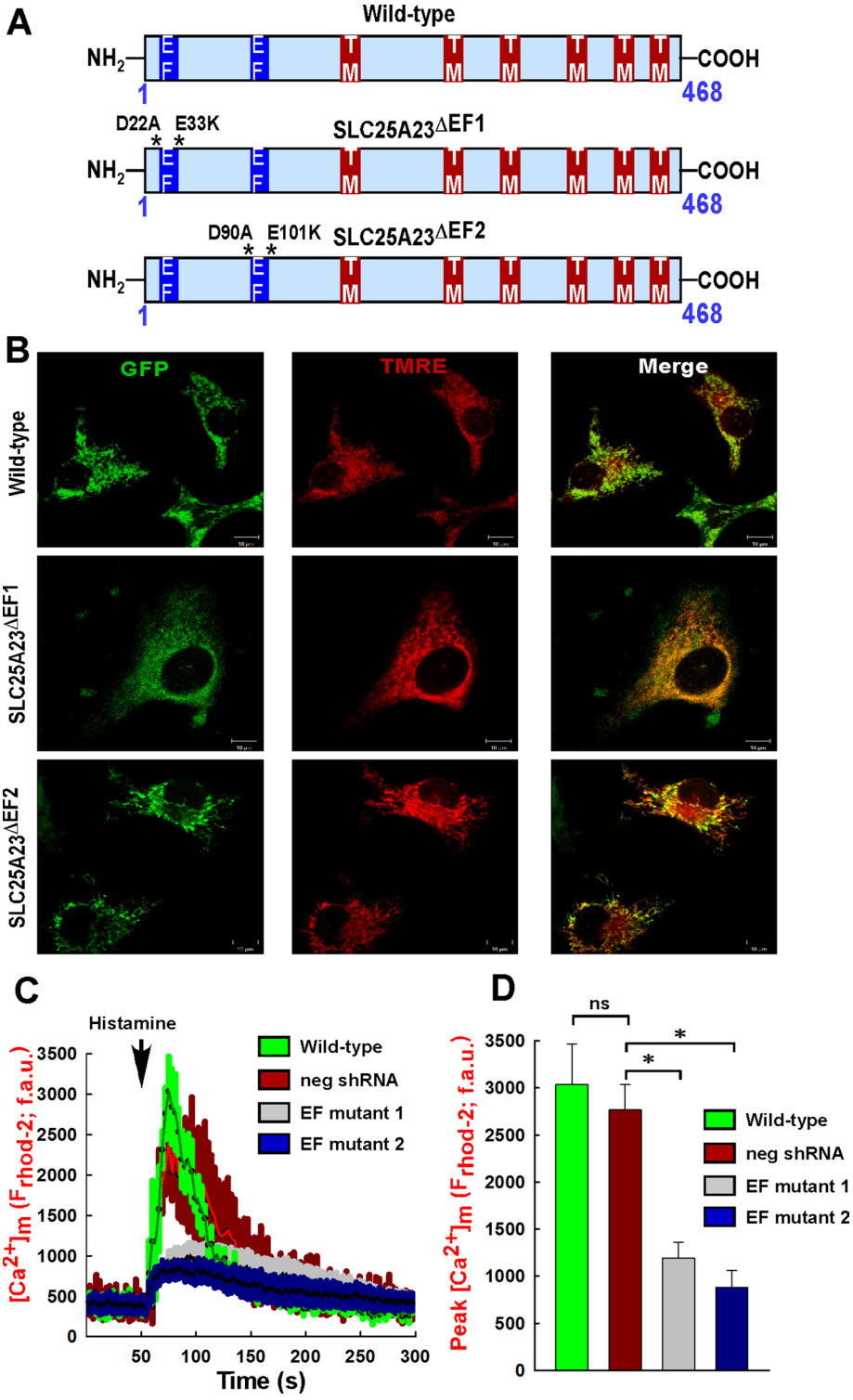

FIGURE 3: SLC25A23 EF-hand mutants dampen mitochondrial Ca^{2+} uptake. (A) Scheme depicting EF1 and EF2 mutant constructs. (B) HeLa cells were transfected with EF-hand mutants, and localization to the mitochondria was visualized with mitochondrial indicator TMRE. (C) EF1 and EF2 mutants show decreased mitochondrial Ca^{2+} uptake assessed by confocal imaging after histamine stimulation. (D) Quantitation of mitochondrial Ca^{2+} peak uptake using mitochondrial Ca^{2+} indicator Rhod-2 AM. Data are mean ± SEM ($n = 3$). *$p < 0.05$ compared with Neg shRNA.

SLC25A23 KD affects mitochondrial ROS production. We assayed for mitochondrial superoxide (mROS) using the mitochondrial targeting superoxide indicator MitoSOX Red. Surprisingly, basal mROS levels were lower in SLC25A23 KD than in control (Figure 6, C and D), and reconstitution of SLC25A23 in clone #864 partially restored the mROS levels (Figure 6, C and D). However, mROS levels in SLC25A24 KD and SLC25A25 KD were similar to those in Neg shRNA cells. We next assessed whether levels of the major antioxidant glutathione changed in SLC25A23 KD cells. Indeed, reduced glutathione levels are higher in SLC25A23 KD (Figure 6, E and F). Together these results demonstrate that knockdown of SLC25A23 has no effect on basal mitochondrial bioenergetics but lowers basal mROS.

Knockdown of SLC25A23 protects cells from oxidative stress

Having observed reduction of mitochondrial Ca^{2+} uptake and mROS production during the basal state, we finally examined whether knockdown of SLC25A23 alleviates cell death during active mitochondrial Ca^{2+}-overload conditions. SLC25A23 knockdown #864 and partial knockdown #863 both exhibited strong global preservation of ATP when compared with negative shRNA after ROS stressors (Figure 7A). Because ATP levels were preserved in the SLC25A23 KD, we performed a cell death assay using *t*-butyl hydroperoxide (t-BH) challenge. Oxidant-treated cells were stained with cell death markers annexin V and propidium iodide and imaged using confocal microscopy. Similar to the observed preservation of ATP levels, SLC25A23 KD was protective against t-BH stress, whereas SLC25A23 #864 rescue exhibited cell death comparable to negative shRNA HeLa cells (Figure 7, B and C). These results establish the role of SLCA25A23 as a link between mitochondrial Ca^{2+} uptake and cell death after oxidative stress.

DISCUSSION

The main finding of our work is that SLC25A23 participates in mitochondrial Ca^{2+} uptake while interacting with key mitochondrial Ca^{2+} uniporter molecules MCU and MICU1. The RNA interference–mediated silencing of SLC25A23 demonstrated SLC25A23's role as a facilitator of mitochondrial Ca^{2+} uptake and mROS production and subsequently alters cell death. In addition, SLC25A23 EF hands are necessary for mitochondrial Ca^{2+} function of SLC25A23.

The MCU channel complex and the mitochondrial solute carriers functionally integrate to create the physiological mitochondrial Ca^{2+} transportome, which comprehensively drives kinetics and maintains equilibrium. Recent findings regarding the interactions of MCU, both distal and proximal, are the emerging focus of mitochondrial biology (Mori *et al.*, 2011; Mallilankaraman *et al.*, 2012a,b). A further example of the signal interaction of MCU and solute carriers is SLC25A12, which is a protein of the mitochondrial inner membrane

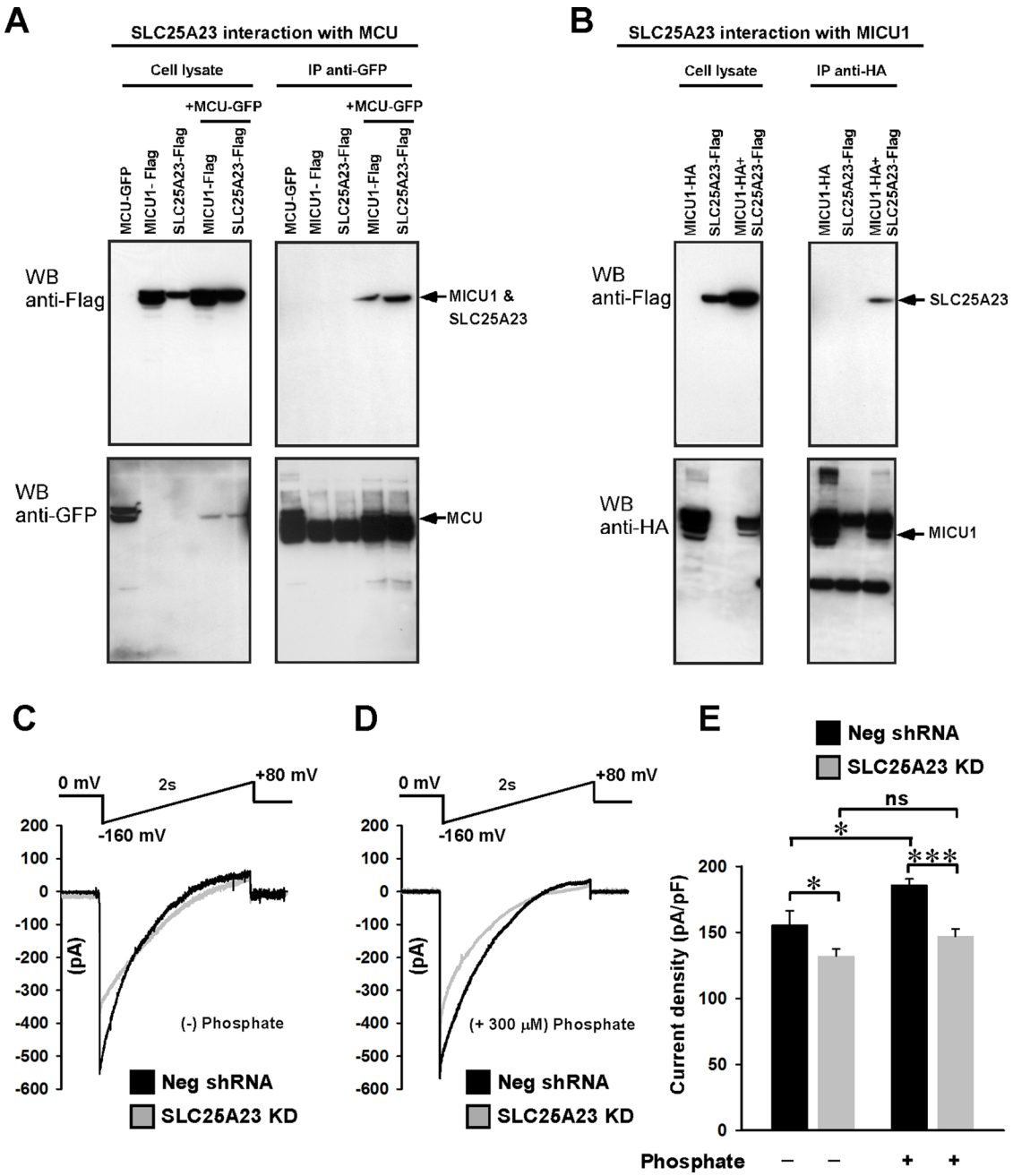

FIGURE 4: SLC25A23 interacts with MCU and MICU1 and modulates I_{MCU}. (A) Stably MCU-GFP–expressing COS7 cells were transfected with Flag-tagged, full-length MICU1 or SLC25A23. After immunoprecipitation with GFP antibody, total cell lysates and immunoprecipitated materials were subjected to Western blot analysis. Cell lysates were probed with anti-Flag (top left) or anti-GFP antibodies (bottom left) to serve as inputs. Immunoprecipitated samples were probed with anti-Flag (top right) or anti-GFP antibodies (bottom right). Anti-GFP antibodies coimmunoprecipitate full-length MICU1 and SLC25A23. $n = 3$. (B) Stably MICU1-HA–expressing COS7 cells were transfected with Flag-tagged SLC25A23. After immunoprecipitation with HA antibody, total cell lysates and immunoprecipitated materials were subjected to Western blot analysis. Cell lysates were probed with anti-Flag (top left) or anti-HA antibodies (bottom left) to serve as inputs. Immunoprecipitated samples were probed with anti-Flag (top right) or anti-HA antibodies (bottom right). Anti-HA antibodies to MICU1-HA coimmunoprecipitate Flag-tagged SLC25A23. $n = 3$. (C) Mitoplast current (I_{MCU}) from HeLa cells was recorded before and after application of 5 mM Ca^{2+} to the bath medium. Currents were measured during a voltage ramp as indicated. Traces are a representative single recording of I_{MCU} from Neg shRNA (black) and SLC25A23 KD (gray). $n = 5$ or 6. (D) Traces are a representative single recording of I_{MCU}. The I_{MCU} was recorded in the presence of 5 mM Ca^{2+} and 300 μM P_i in Neg shRNA (black) and SLC25A23 KD (gray). $n = 6$. (E) I_{MCU} densities (pA/pF) for Neg shRNA (black) and SLC25A23 KD (gray). Mean ± SEM; $*p < 0.05$, $***p < 0.001$; ns, not significant; $n = 5$ or 6.

(del Arco and Satrustegui, 1998) and responds to Ca^{2+} by intermembrane-space EF hands (Pardo *et al.*, 2006; Marmol *et al.*, 2009). In this case, the direct Ca^{2+}-induced function of SLC25A12 is to increase mitochondrial levels of NAD(P)H (Satrustegui *et al.*, 2007a; Wibom *et al.*, 2009). In addition, correlative gene expression analysis in cancer cell lines strongly supports our conclusion that SLC25A23 Ca^{2+}

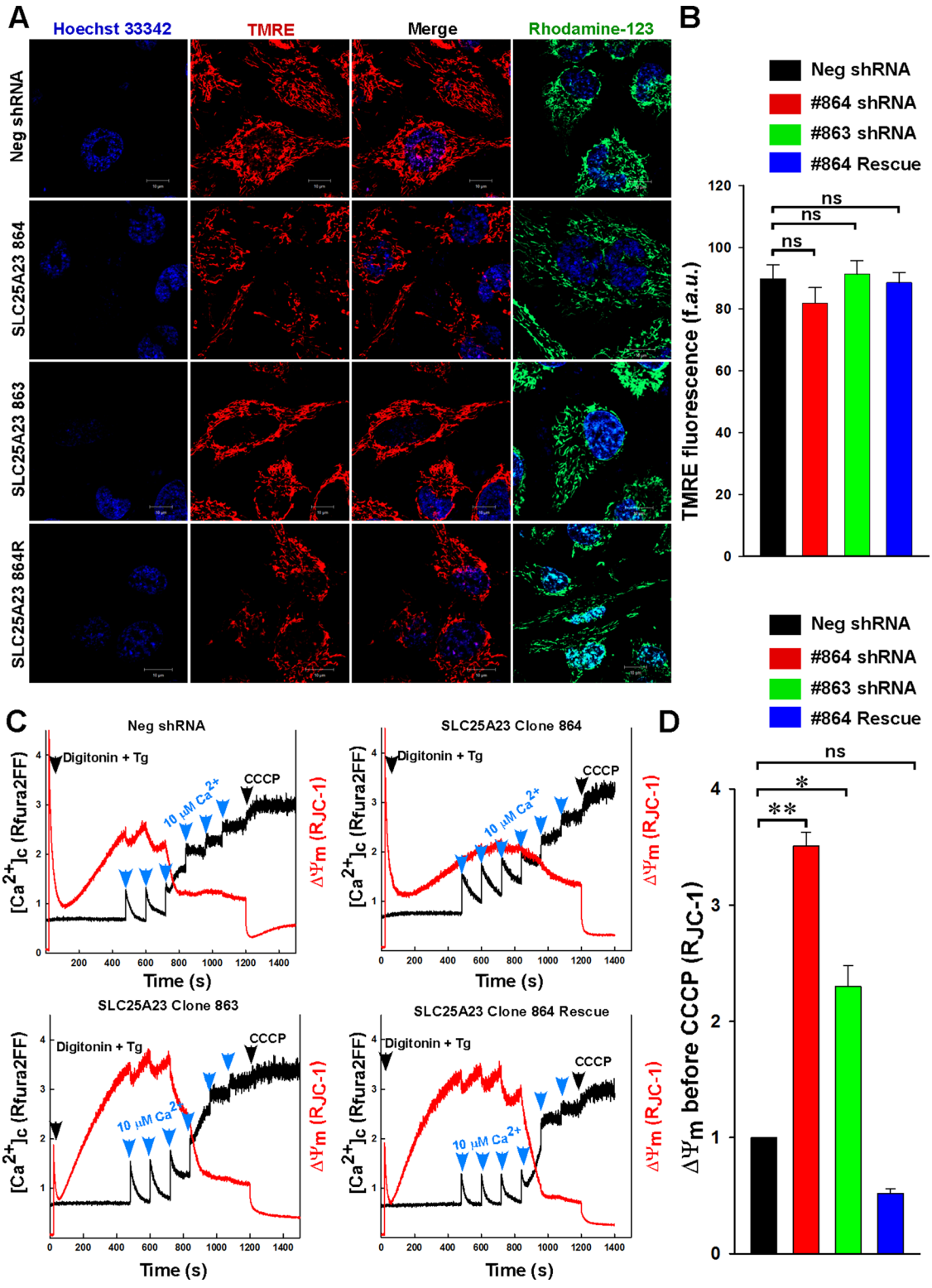

FIGURE 5: SLC25A23 knockdown prevents mitochondrial Ca^{2+} uptake and subsequently preserves $\Delta\Psi_m$. (A) Mitochondrial morphology and $\Delta\Psi_m$ was assessed by confocal microscopy using TMRE and rhodamine 123. Hoechst 33342 was used as a nuclear marker. (B) Quantitation of confocal TMRE fluorescence. (C) Representative traces of permeabilized (40 μg/ml digitonin) HeLa cells loaded with the ratiometric Ca^{2+} indicator Fura-2FF and ratiometric $\Delta\Psi_m$ fluorophore JC-1 and pulsed with 10 μM Ca^{2+} to trigger $\Delta\Psi_m$ loss, followed by addition of the uncoupler CCCP (1 μM). $\Delta\Psi_m$ loss was similar between Neg shRNA control and partial knockdown clone 863. Clone 864 shows abrogated $\Delta\Psi_m$ loss after six Ca^{2+} pulses, and the first pulse is not completely cleared from the cytosol. (D) Quantitation after the addition of the uncoupler CCCP shows $\Delta\Psi_m$ preservation in clone 864. Data are mean ± SEM (n = 3–5). *p < 0.05, **p < 0.01, and ns, not significant compared with Neg shRNA.

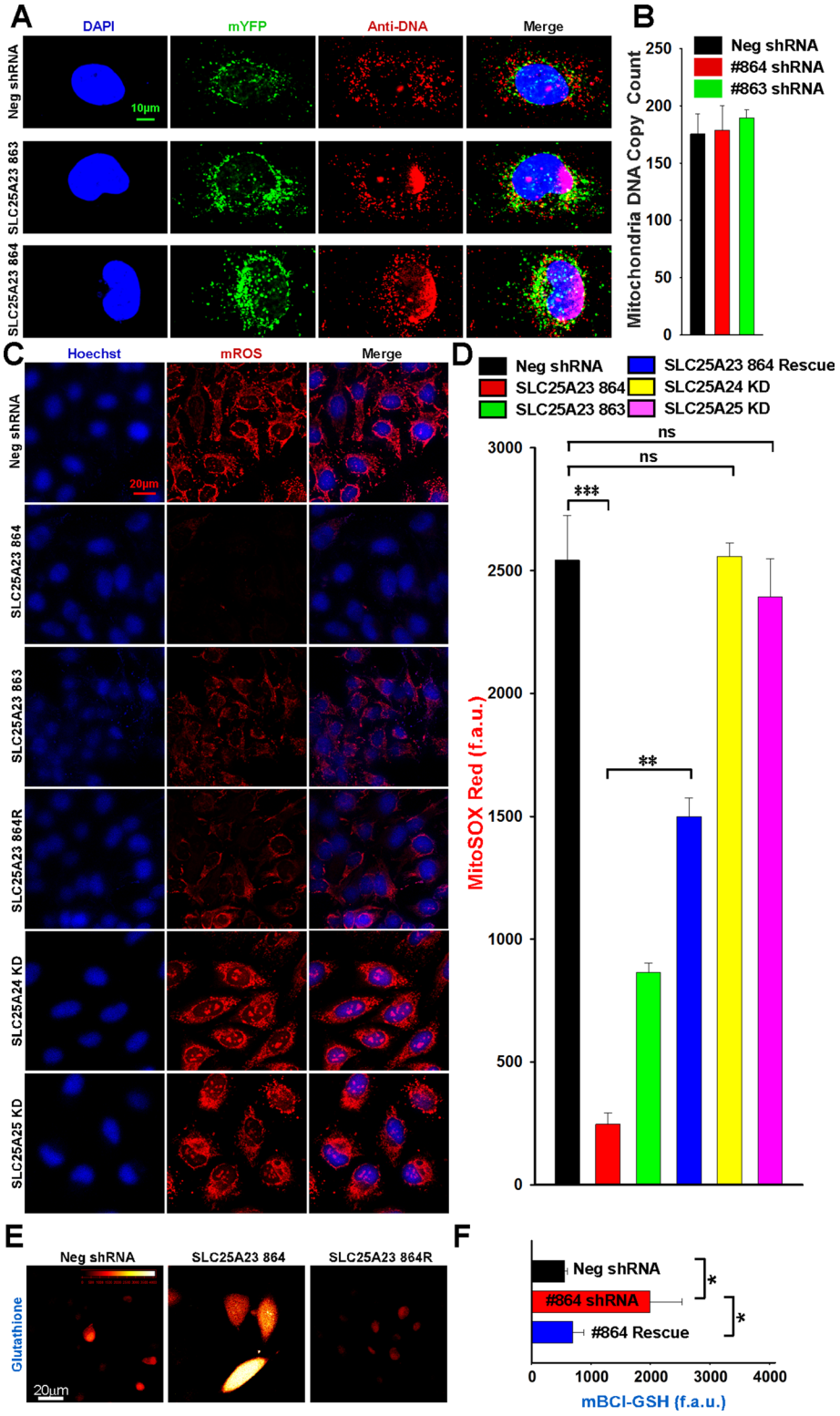

FIGURE 6: Knockdown of SLC25A23 lowers basal mitochondrial ROS production. (A) HeLa cells were transfected with mito-GFP (green), and cells were immunostained with anti-DNA antibody (red). Images were acquired using a Zeiss LSM 710 META NLO imaging system. Representative images of Neg shRNA (top), clone 863 (middle), and clone 864 (bottom). (B) Quantitation of total mitochondrial anti-DNA spots per cell as determined by ImageJ Particle Analyzer counting all resolvable (>0.37 μm) binary-colored particles. (C) HeLa cells were loaded with the mitochondrial superoxide indicator MitoSOX Red and the nuclear marker Hoechst 33342. (D) Quantitation of MitoSOX Red fluorescence. (E) HeLa cells were loaded with the reduced glutathione indicator monochlorobimane (mBCl) and imaged using a Zeiss LSM 510 with 405-nm excitation. (F) Quantitation of mBCl-GSH fluorescence. Data are mean ± SEM ($n = 3$). *$p < 0.05$, **$p < 0.01$, ***$p < 0.001$ compared with #864 shRNA or Neg shRNA.

uptake plays a role in ROS-dependent cell death but does not alter mitochondrial bioenergetics (Huang *et al.*, 2004). Further, SLC25A23, SLC25A37, and SLC25A4 were implicated in cancer-related fatigue, a major quality-of-life determinant (Hsiao *et al.*, 2013).

Surprisingly, not only does SLC25A23 functionally regulate MCU Ca^{2+} influx, possibly by Ca^{2+}-activated phosphate anion flow, which balances the net charge of matrix ion influx, but also the multipass transmembrane SLC25A23 interacts with MCU, perhaps due to hydrophobic interactions in the transmembrane portions. SLC25A23 interaction with MICU1 may be indirect through MCU, or SLC25A23 could sequester MICU1, thus increasing I_{MCU}. The functional regulation of MCU by SLC25A23 and the biophysical characterization of SLC25A23/MCU/MICU1 complex need further investigation. Our results show evidence of SLC25A23 interaction with MCU and functional I_{MCU} modulation of MCU by SLC25A23, suggesting a supercomplex integrating channels and carriers in microdomains for enhanced sensitivity. In support of this concept, a recent SILAC MS/MS study identified SLC25A3 (phosphate carrier; Palmieri, 2004) as a possible MCU transportome component in the 293T cell line (Sancak *et al.*, 2013). Although SLC25A23 was not detected in this pull-down approach (Sancak *et al.*, 2013), it is possible that cell type and the solute carrier conserved domain are key factors in solute carrier/MCU interaction. SLC25A23 expression was reported to be nominal in kidney (293T is a human embryonic kidney epithelial cell line) and other tissues as compared with brain and liver (Traba *et al.*, 2012). Together these findings suggest that rigorous interaction studies are warranted to define the MCU supercomplex. Although we show that MCU-mediated Ca^{2+} uptake interacts with the function of SLC25A23, the two systems are distinct, as SLC25A23 is derived from a separate lineage (Bick *et al.*, 2012). However, both MCU and SLC25A23 have orthologues extending back to the common

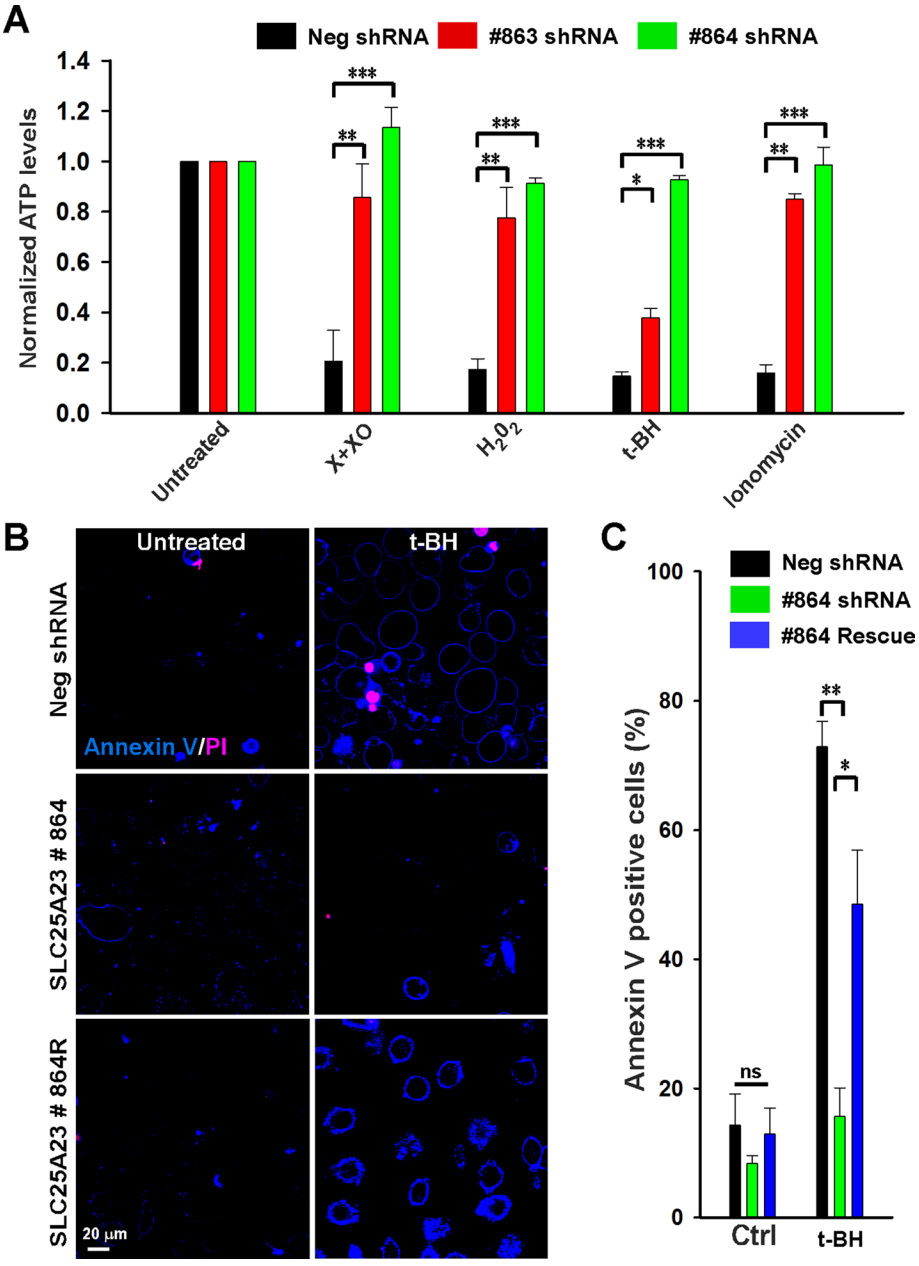

FIGURE 7: Knockdown of SLC25A23 preserves cellular ATP levels and cell viability. (A) Knockdown of SLC25A23 preserves ATP levels after oxidant challenge. HeLa cells (Neg shRNA, 863, and 864) were challenged with superoxide generation system (xanthine + xanthine oxidase), hydrogen peroxide (H_2O_2), *t*-butyl hydroperoxide, or ionomycin. After 6 h, cellular ATP levels were assessed using the CellTiter-Glo Luminescent kit. (B) HeLa cells (Neg shRNA, #863, and #864) were treated with *t*-butyl hydroperoxide for 6 h and then stained with the cell death markers annexin V and propidium iodide. (C) Quantitation of annexin V–positive staining. Data are mean ± SEM ($n = 3$). *$p < 0.05$, **$p < 0.01$, and ***$p < 0.001$, and ns, not significant compared with Neg shRNA or #864 shRNA.

ancestor of eukaryotes, suggesting the possibility of coevolution (Flicek *et al.*, 2013).

Mitochondrial Ca^{2+} overload often results in loss of $\Delta\Psi_m$, causing bioenergetic collapse (Bernardi *et al.*, 1999; Rizzuto *et al.*, 2012). SLC25A23 silencing preserved $\Delta\Psi_m$ while reducing Ca^{2+} uptake after GPCR stimulation. In addition, we found that SLC25A23 has a ROS-dependent cell death function, as knockdown of SLC25A23 preserves ATP, indicative of maintained $\Delta\Psi_m$, intact proton pumping, and decreased cell death. In particular, the enhanced survival after t-BT is especially significant, as t-BH induction of cell death requires Ca^{2+} (Crompton and Costi, 1988) and can be rescued by ethylene glycol tetraacetic acid (EGTA) (Crompton *et al.*, 1987), establishing a link through SLC25A23 from Ca^{2+} to t-BH–induced cell death.

Our results as a whole demonstrate that SLC25A23 enhances mitochondrial Ca^{2+} uptake. Functionally, SLC25A23 senses Ca^{2+} after GPCR stimulation and provides a response that enhances MCU-mediated mitochondrial Ca^{2+} uptake. Since the identification of mitochondrial Ca^{2+} current (Kirichok *et al.*, 2004), several molecules, including uncoupling proteins 2 and 3 (Trenker *et al.*, 2007), LETM1 (Jiang *et al.*, 2009), MICU1 (Perocchi *et al.*, 2010; Mallilankaraman *et al.*, 2012b; Hoffman *et al.*, 2013), MCU (Baughman *et al.*, 2011; De Stefani *et al.*, 2011), MCUR1 (Mallilankaraman *et al.*, 2012a), MICU2 (Plovanich *et al.*, 2013), MCUb (Raffaello *et al.*, 2013), and EMRE (Sancak *et al.*, 2013), have been described as mitochondrial Ca^{2+} signal integrators. In total, our study reveals SLC25A23 as a mitochondrial Ca^{2+}-uptake regulator with significant ROS and cell death implications, providing a mechanism for targeting of MCU-dependent Ca^{2+} overload.

MATERIALS AND METHODS

Ca^{2+} uptake and $\Delta\Psi_m$ measurement in permeabilized cell system

Mitochondrial Ca^{2+} uptake and $\Delta\Psi_m$ were determined by simultaneous monitoring of cytosolic Ca^{2+} with Fura-2FF (0.5 μM; Life Technologies, Grand Island, NY) and $\Delta\Psi_m$ with the lipophilic cationic dye 5,5′,6,6′-tetrachloro-3,3′-tetraethylbenzimidazolcarbocyanine (JC-1; 800 nM; Life Technologies) changes. Cells grown in T-75 flasks were trypsinized, neutralized with fetal bovine serum, centrifuged at 1500 rpm for 5 min, aspirated, resuspended in 20 ml of phosphate-buffered saline, centrifuged at 800 rpm for 3 min, aspirated, and then resuspended in ICM buffer containing 40 μg/ml digitonin to permeabilize the cells, protease inhibitors (EDTA-free cOMPLETE tablets; Roche Applied Science, Indianapolis, IN), and 2 μM thapsigargin to block the SERCA pump. Mitochondria were energized with 2 mM of succinate (Hawkins *et al.*, 2010b), and then 8×10^6 cells were resuspended in 1 ml of ICM buffer and followed by Fura-2FF as a cytosolic Ca^{2+} indicator. After 20 s of data recording, JC-1 was added. At 480 s and every 120 s thereafter, 10 μM Ca^{2+} was added. CCCP, 2 μM, was added at 1200 s. Fluorescence was measured using a dual-wavelength fluorimeter (PTI) with 490-nm excitation and 535-nm emission for monomeric JC-1 and 570/595 nm for the J-aggregate. The $\Delta\Psi_m$ was calculated as the ratio of J-aggregate and the monomer (Irrinki *et al.*, 2011).

Cell culture

HeLa cells were cultured using low-glucose DMEM (GIBCO, Life Technologies) containing 10% fetal bovine serum and 1% penicillin/streptomycin, with or without 2 µg/ml puromycin and with or without G418 (500 µg/ml). For each isoform—SLC25A23, SLC25A24, and SLC25A25—five shRNA constructs were expressed.

Generation of stable SLC25A23, SLC25A24, and SLC25A25 shRNA knockdown and rescue HeLa cell clones

The following shRNA sequences were obtained from Open Biosystems, Pittsburgh, PA: for SLC25A23, #863, CCTGAATCTTAGACTCTTATA; #864, CGAGTCAGCTATCAAGTTCAT; #865, CGGCTGAACAGAATCGTTCAA; #866, CGTCTACGAGACTCTGAAGAA; and #867, CTGCTCATGTTTCACAGTCTT; for SLC25A24, #592, GACACTGGGTCTGACTATTTC; #593, TATTAGGTATCATACCTTATG; #594, TGGCCTCTTTCGACGAATTAT; #595, TTCGGGTGGTTTACGTTTATG; and #720 ATGAGCTCTTGAAGTCCTATT; and for SLC25A25, #736, AGACCGAGTTCCAGTACTTTG; #737, CTGCCGAGCTGAAGTCCATTT; #738, GGGACTTGGGAGTCAAGATAT; #739, CCCGAATCAGCCATCAAATTC; and #740 CCCTCGTCCAATCCCATAATC. HeLa cells (5×10^5/well) grown in six-well plates were transduced with the lentivirus for knockdown. Two days posttransduction, the cells were selected with puromycin (2 mg/ml) for 6–10 d and expanded. For the rescue studies, a SLC25A23 construct resistant to #864 shRNA knockdown was created (OriGene Technologies, Rockville, MD). The rescue plasmid encoding SLC25A23 cDNA harbored four silent point mutations in the region complementary to SLC25A23 shRNA. The #864 knockdown cells were transfected with SLC25A23 rescue construct, and the knockdown cells expressing shRNA-resistant SLC25A23 cDNAs were selected with 500 µg/ml G418 (Life Technologies).

qRT PCR analysis

The knockdown and overexpression were assessed by qRT PCR. Briefly, total RNA was isolated from HeLa wild type (WT), Neg shRNA, SLC25A23 KD, SLC25A24 KD, and SLC25A25 KD and rescue cells, using the RNeasy Mini Kit (Qiagen, Valencia, CA) in accordance with the manufacturer's instructions. Total RNA (1 µg) was reverse transcribed with the Verso cDNA Kit (Abgene, Cambridge, United Kingdom). Real-time qPCRs were performed with the gene-specific Solaris qPCR gene expression assay kit (Abgene) as per the manufacturer's instructions. (SLC25A23: forward primer, AACAGGGTATCTCCTCTGAG, reverse primer, AGTCTTGACCGGAACCAG, and probe, AGTCTTGACCGGAACCAG; SLC25A24: forward primer, ATGCAGGCTCAAGCCATGT, reverse primer, GCCTCTGTAAAGTCCTGGTA, and probe, TCCAAAGAAGGAATACC; and SLC25A25: forward primer, TGGAAGCATTCCACGATCT, reverse primer, TGAACTCATCCGGGACCGTTA, and probe, ATGTGGGTGAGAATCTA). The relative gene expression was calibrated with WT type using 7300 Real Time PCR system RQ study software (Applied Biosystems, Carlsbad, CA).

Cytosolic and mitochondrial Ca^{2+} dynamics

HeLa cells were grown on 25-mm glass coverslips for 48 h and loaded with 2 µM Rhod-2 AM (50 min) and 5 µM Fluo-4 AM (30 min) (Life Technologies) in extracellular medium (Madesh *et al.*, 2005; Mallilankaraman *et al.*, 2012a). After 1 min of baseline recording, agonist (histamine, 100 µM) was added, and confocal images were recorded every 3 s (510 Meta; Carl Zeiss, Thornwood, NY) at 488- and 561-nm excitation using a 63× oil objective to simultaneously monitor cytoplasmic and mitochondrial Ca^{2+} dynamics. Images were analyzed and quantified using ImageJ (National Institutes of Health, Bethesda, MD) and custom-made software (Spectralyzer, Elmsford, NY).

Assessment of mitochondrial Ca^{2+} influx and efflux rates

HeLa cells were permeabilized and loaded with the ratiometric Ca^{2+} indicator Fura2-FF. Cells were pulsed with 10 µM Ca^{2+} at 350 s to measure mitochondrial Ca^{2+} uptake, followed by addition of 1 µM Ru360 at 550 s, 10 µM CGP37157 at 610 s, and 2 µM CCCP at 750 s.

Coimmunoprecipitation assay

Cell extracts were prepared from either stably or transiently transfected COS-7 cells using RIPA buffer (50 mM Tris-HCl, pH 7.4, 150 mM NaCl, 0.25% deoxycholic acid, 1 mM EDTA, 1% NP-40, protease inhibitor cocktail [Complete; Roche, Indianapolis, IN], and 1 mM phenylmethylsulfonyl fluoride). To study the interaction of MCU with SLC25A23, we used GFP-tagged MCU and Flag-tagged SLC25A23. Flag-tagged MICU1 was used as a positive control (Hoffman *et al.*, 2013). Stably MCU-GFP–expressing COS7 cells were transfected with Flag-tagged, full-length MICU1 or SLC25A23. Similarly for understanding the interaction of SLC25A23 with MICU1, stably MICU1-HA–expressing COS7 cells were transfected with Flag-tagged SLC25A23. After immunoprecipitation with anti-GFP (Evrogen, Moscow, Russia) or anti-HA (Thermo Scientific, Waltham, MA) antibody, total cell lysates and immunoprecipitated materials were subjected to Western blot analysis. Ten percent of cell lysates were probed with anti-Flag (Sigma-Aldrich, St. Louis, MO), anti-GFP or anti-HA antibodies to serve as inputs, and similarly, immunoprecipitated samples were probed with their corresponding antibodies.

I_{MCU} recording

Mitoplast patch clamp recordings were conducted at 30°C as previously described (Kirichok *et al.*, 2004; Hoffman *et al.*, 2013). I_{MCU} was recorded using a computer-controlled Axon200B patch-clamp amplifier with a Digidata 1320A acquisition board (pClamp 10.0 software; Axon Instruments, Sunnyvale, CA). Mitoplasts were bathed in $CaCl_2$ (5 mM) ± P_i (300 µM), sodium gluconate (150 mM), KCl (5.4 mM), and 4-(2-hydroxyethyl)-1-piperazineethanesulfonic acid (HEPES; 10 mM), pH 7.2. The pipette solution contained sodium gluconate (150 mM), NaCl (5 mM), sucrose (135 mM), HEPES (10 mM), and EGTA (1.5 mM), pH 7.2. After formation of GΩ seals (pipette resistance, 15–25 MΩ), the mitoplasts were ruptured with 200- to 400-mV pulses varying from 2- to 6-ms duration. Mitoplast capacitance was measured (2.2–3.8 pF). After capacitance compensation, mitoplasts were held at 0 mV, and I_{MCU} was elicited with a voltage ramp (from –160 to 80 mV, 120 mV/s).

Oxygen consumption rate

HeLa cells (1×10^6) were permeabilized with 20 µg/ml digitonin in 140 µl of intracellular medium (120 mM KCl, 10 mM NaCl, 1 mM KH_2PO_4, 20 mM HEPES–Tris, pH 7.2), and oxygen consumption rate was measured using a MT200A MitoCell Clark-type electrode and MT200A MitoCell chamber (Strathkelvin Instruments, Motherwell, United Kingdom) during constant stirring (Irrinki *et al.*, 2011). Next, in 1-min intervals, 5 mM complex I substrates malate/pyruvate, 100 nM complex I inhibitor rotenone, 5 mM complex II substrate succinate, 50 nM complex II inhibitor antimycin A, 0.4 mM complex V substrates tetramethylphenylenediamine/2.5 mM ascorbate, and 1 µM complex IV inhibitor sodium azide were added (Irrinki *et al.*, 2011).

NAD(P)H autofluorescence measurement

NAD(P)H autofluorescence was measured through the change in autofluorescence of NAD(P)H at 350/460 nm (excitation/emission)

with a multiwavelength-excitation, dual-wavelength-emission fluorimeter (Delta RAM; PTI, Birmingham, NJ; Jones *et al.*, 2007). Briefly, cells (8×10^6 cells) were suspended in Hank's balanced salt solution (Sigma-Aldrich) and permeabilized with digitonin (Hawkins *et al.*, 2010b). NAD(P)H levels were monitored before and after 10 μM rotenone.

Confocal $\Delta\Psi_m$ measurement

HeLa cells were plated in six-well plates containing 0.2% gelatin–coated glass coverslips (Thapa *et al.*, 2011), and 100 nM TMRE perchlorate was added to cells and incubated for 30 min at 37°C. Nuclear DNA stain, 2-(4-ethoxyphenyl)-6-[6-(4-methylpiperazin-1-yl)-1H-benzimidazol-2-yl]-1H-benzimidazole (Hoescht 33342), was added for 5 min. Image acquisition was performed using a Carl Zeiss 510 confocal microscope using a 63× oil objective with excitation at 561 and 405 nm, respectively. Images were quantified using ImageJ (Madesh *et al.*, 2005).

Mitochondrial ROS measurement

HeLa cells were loaded with the mitochondrial superoxide–sensitive fluorophore MitoSOX Red (Life Technologies; 10 μM) in extracellular matrix (ECM) containing 2% bovine serum albumin (BSA) at 37°C for 10 min. Cells were incubated with Hoescht 33342 for an additional 5 min at room temperature. Cells were then washed, resuspended in ECM containing 0.2% BSA, and imaged using a Carl Zeiss 710 two-photon confocal microscope with a 20× liquid immersion objective at 405 and 561 nm for Hoescht 33342 and MitoSOX Red, respectively (Robinson *et al.*, 2006; Mukhopadhyay *et al.*, 2007).

Mitochondrial DNA content measurement

HeLa cells were transiently transfected with the mitochondrial marker monomeric yellow fluorescent protein plasmid construct. After 48 h, cells were fixed and stained for mitochondrial DNA using monoclonal anti-DNA antibody conjugated with secondary goat anti-mouse immunoglobulin M–Alexa Fluor 594 (Life Technologies). Slides were mounted using ProLong Gold Antifade reagent (Molecular Probes). Images were acquired using a Carl Zeiss 710 two-photon confocal microscope with a 63× oil objective. mtDNA was quantified using ImageJ software.

ATP measurement

ATP levels were measured using the CellTiter-Glo Luminescent Cell Viability Assay (Promega, Madison, WI) as per the manufacturer's instructions. ATP levels (luminescence) were measured in a model 96F nontreated white microwell plate (Nunc, Rochester, NY) using a Victor X5 2030 multilabel reader (Perkin Elmer, Waltham, MA; Irrinki *et al.*, 2011). To verify loading quantity, a Bradford assay was performed.

Assessment of cell death

HeLa cells were challenged with *t*-butyl hydroperoxide (200 μM). After treatment, the cells were labeled with annexin V–Alexa 405 conjugate for 25 min with annexin binding buffer (Molecular Probes, Life Technologies). During annexin V binding, propidium iodide (0.5 μg/ml) was also loaded to visualize plasma membrane integrity. Cell death was monitored using a Carl Zeiss 510 Meta confocal imaging system (Madesh *et al.*, 2002, 2005, 2009).

Statistical analysis

All experiments were performed three or more times. Data from multiple experiments were quantified and are expressed as mean ± SEM, and differences between groups were analyzed by using a two-tailed Student's *t* test. $p < 0.05$ was considered significant in all analyses. Data were plotted with either GraphPad Prism (La Jolla, CA), version 5.0, or SigmaPlot 11.0 software.

ACKNOWLEDGMENTS

We thank Xianhua Wang and Heping Cheng for sharing the GCaMP2-mt plasmid construct. We also thank Donald L. Gill, Dale Haines, and Jonathan Soboloff for their comments. This work was supported by National Institutes of Health Grants HL086699, HL086699-01A2S1, and 1S10RR027327-01 to M.M.

REFERENCES

Amigo I, Traba J, Gonzalez-Barroso MM, Rueda CB, Fernandez M, Rial E, Sanchez A, Satrustegui J, Del Arco A (2013). Glucagon regulation of oxidative phosphorylation requires an increase in matrix adenine nucleotide content through Ca2+ activation of the mitochondrial ATP-Mg/Pi carrier SCaMC-3. J Biol Chem 288, 7791–7802.

Anunciado-Koza RP, Zhang J, Ukropec J, Bajpeyi S, Koza RA, Rogers RC, Cefalu WT, Mynatt RL, Kozak LP (2011). Inactivation of the mitochondrial carrier SLC25A25 (ATP-Mg2+/Pi transporter) reduces physical endurance and metabolic efficiency in mice. J Biol Chem 286, 11659–11671.

Aprille JR (1988). Regulation of the mitochondrial adenine nucleotide pool size in liver: mechanism and metabolic role. FASEB J 2, 2547–2556.

Bassi MT, Manzoni M, Bresciani R, Pizzo MT, Della Monica A, Barlati S, Monti E, Borsani G (2005). Cellular expression and alternative splicing of SLC25A23, a member of the mitochondrial Ca2+-dependent solute carrier gene family. Gene 345, 173–182.

Baughman JM *et al.* (2011). Integrative genomics identifies MCU as an essential component of the mitochondrial calcium uniporter. Nature 476, 341–345.

Bernardi P, Scorrano L, Colonna R, Petronilli V, Di Lisa F (1999). Mitochondria and cell death. Mechanistic aspects and methodological issues. Eur J Biochem 264, 687–701.

Bick AG, Calvo SE, Mootha VK (2012). Evolutionary diversity of the mitochondrial calcium uniporter. Science 336, 886.

Carafoli E, Lehninger AL (1971). A survey of the interaction of calcium ions with mitochondria from different tissues and species. Biochem J 122, 681–690.

Cox DA, Conforti L, Sperelakis N, Matlib MA (1993). Selectivity of inhibition of Na(+)-Ca2+ exchange of heart mitochondria by benzothiazepine CGP-37157. J Cardiovasc Pharmacol 21, 595–599.

Crompton M, Costi A (1988). Kinetic evidence for a heart mitochondrial pore activated by Ca2+, inorganic phosphate and oxidative stress. A potential mechanism for mitochondrial dysfunction during cellular Ca2+ overload. Eur J Biochem 178, 489–501.

Crompton M, Costi A, Hayat L (1987). Evidence for the presence of a reversible Ca2+-dependent pore activated by oxidative stress in heart mitochondria. Biochem J 245, 915–918.

Davidson SM, Duchen MR (2012). Imaging mitochondrial calcium signalling with fluorescent probes and single or two photon confocal microscopy. Methods Mol Biol 810, 219–234.

De Stefani D, Raffaello A, Teardo E, Szabo I, Rizzuto R (2011). A forty-kilodalton protein of the inner membrane is the mitochondrial calcium uniporter. Nature 476, 336–340.

del Arco A, Satrustegui J (1998). Molecular cloning of aralar, a new member of the mitochondrial carrier superfamily that binds calcium and is present in human muscle and brain. J Biol Chem 273, 23327–23334.

del Arco A, Satrustegui J (2004). Identification of a novel human subfamily of mitochondrial carriers with calcium-binding domains. J Biol Chem 279, 24701–24713.

Dransfield DT, Aprille JR (1993). Regulation of the mitochondrial ATP-Mg/Pi carrier in isolated hepatocytes. Am J Physiol 264, C663–C670.

Fiermonte G, De Leonardis F, Todisco S, Palmieri L, Lasorsa FM, Palmieri F (2004). Identification of the mitochondrial ATP-Mg/Pi transporter. Bacterial expression, reconstitution, functional characterization, and tissue distribution. J Biol Chem 279, 30722–30730.

Flicek P *et al.* (2013). Ensembl 2013. Nucleic Acids Res 41, D48–D55.

Hajnoczky G, Csordas G, Das S, Garcia-Perez C, Saotome M, Sinha Roy S, Yi M (2006). Mitochondrial calcium signalling and cell death: approaches for assessing the role of mitochondrial Ca2+ uptake in apoptosis. Cell Calcium 40, 553–560.

Hawkins BJ *et al.* (2010a). S-glutathionylation activates STIM1 and alters mitochondrial homeostasis. J Cell Biol 190, 391–405.

Hawkins BJ, Levin MD, Doonan PJ, Petrenko NB, Davis CW, Patel VV, Madesh M (2010b). Mitochondrial complex II prevents hypoxic but not calcium- and proapoptotic Bcl-2 protein-induced mitochondrial membrane potential loss. J Biol Chem 285, 26494–26505.
Haynes RC Jr, Picking RA, Zaks WJ (1986). Control of mitochondrial content of adenine nucleotides by submicromolar calcium concentrations and its relationship to hormonal effects. J Biol Chem 261, 16121–16125.
Hoffman NE *et al.* (2013). micu1 motifs define mitochondrial calcium uniporter binding and activity. Cell Rep 5, 1576–1588.
Hom J, Yu T, Yoon Y, Porter G, Sheu SS (2010). Regulation of mitochondrial fission by intracellular Ca2+ in rat ventricular myocytes. Biochim Biophys Acta 1797, 913–921.
Hsiao CP, Wang D, Kaushal A, Saligan L (2013). Mitochondria-related gene expression changes are associated with fatigue in patients with non-metastatic prostate cancer receiving external beam radiation therapy. Cancer Nurs 36, 189–197.
Huang Y, Anderle P, Bussey KJ, Barbacioru C, Shankavaram U, Dai Z, Reinhold WC, Papp A, Weinstein JN, Sadee W (2004). Membrane transporters and channels: role of the transportome in cancer chemosensitivity and chemoresistance. Cancer Res 64, 4294–4301.
Iijima M, Yamamoto J, Takada N, Ohata H, Momose K (2001). Changes in Ca2+ signaling and contractile protein isoforms in smooth muscle cells from guinea pig ileum during culture. J Smooth Muscle Res 37, 53–66.
Irrinki KM *et al.* (2011). Requirement of FADD, NEMO, and BAX/BAK for aberrant mitochondrial function in tumor necrosis factor alpha-induced necrosis. Mol Cell Biol 31, 3745–3758.
Jiang D, Zhao L, Clapham DE (2009). Genome-wide RNAi screen identifies Letm1 as a mitochondrial Ca2+/H+ antiporter. Science 326, 144–147.
Jones RG *et al.* (2007). The proapoptotic factors Bax and Bak regulate T Cell proliferation through control of endoplasmic reticulum Ca(2+) homeostasis. Immunity 27, 268–280.
Kirichok Y, Krapivinsky G, Clapham DE (2004). The mitochondrial calcium uniporter is a highly selective ion channel. Nature 427, 360–364.
Kucejova B, Li L, Wang X, Giannattasio S, Chen XJ (2008). Pleiotropic effects of the yeast Sal1 and Aac2 carriers on mitochondrial function via an activity distinct from adenine nucleotide transport. Mol Genet Genomics 280, 25–39.
Madesh M, Antonsson B, Srinivasula SM, Alnemri ES, Hajnoczky G (2002). Rapid kinetics of tBid-induced cytochrome c and Smac/DIABLO release and mitochondrial depolarization. J Biol Chem 277, 5651–5659.
Madesh M, Hajnoczky G (2001). VDAC-dependent permeabilization of the outer mitochondrial membrane by superoxide induces rapid and massive cytochrome c release. J Cell Biol 155, 1003–1015.
Madesh M, Hawkins BJ, Milovanova T, Bhanumathy CD, Joseph SK, Ramachandrarao SP, Sharma K, Kurosaki T, Fisher AB (2005). Selective role for superoxide in InsP3 receptor-mediated mitochondrial dysfunction and endothelial apoptosis. J Cell Biol 170, 1079–1090.
Madesh M *et al.* (2009). Execution of superoxide-induced cell death by the proapoptotic Bcl-2-related proteins Bid and Bak. Mol Cell Biol 29, 3099–3112.
Mallilankaraman K *et al.* (2012a). MCUR1 is an essential component of mitochondrial Ca(2+) uptake that regulates cellular metabolism. Nat Cell Biol 14, 1336–1343.
Mallilankaraman K *et al.* (2012b). MICU1 is an essential gatekeeper for MCU-mediated mitochondrial Ca(2+) uptake that regulates cell survival. Cell 151, 630–644.
Marmol P, Pardo B, Wiederkehr A, del Arco A, Wollheim CB, Satrustegui J (2009). Requirement for aralar and its Ca2+-binding sites in Ca2+ signal transduction in mitochondria from INS-1 clonal beta-cells. J Biol Chem 284, 515–524.
Molinari F *et al.* (2009). Mutations in the mitochondrial glutamate carrier SLC25A22 in neonatal epileptic encephalopathy with suppression bursts. Clin Genet 76, 188–194.
Molinari F *et al.* (2005). Impaired mitochondrial glutamate transport in autosomal recessive neonatal myoclonic epilepsy. Am J Hum Genet 76, 334–339.
Mori Y, Kiyonaka S, Kanai Y (2011). Transportsomes and channelsomes: are they functional units for physiological responses. Channels (Austin) 5, 387–390.
Mukhopadhyay P, Rajesh M, Hasko G, Hawkins BJ, Madesh M, Pacher P (2007). Simultaneous detection of apoptosis and mitochondrial superoxide production in live cells by flow cytometry and confocal microscopy. Nat Protoc 2, 2295–2301.
Nicholls DG (2005). Mitochondria and calcium signaling. Cell Calcium 38, 311–317.
Nosek MT, Dransfield DT, Aprille JR (1990). Calcium stimulates ATP-Mg/Pi carrier activity in rat liver mitochondria. J Biol Chem 265, 8444–8450.
Palmieri F (2004). The mitochondrial transporter family (SLC25): physiological and pathological implications. Pflugers Arch 447, 689–709.
Palmieri F (2013). The mitochondrial transporter family SLC25: identification, properties and physiopathology. Mol Aspects Med 34, 465–484.
Palmieri L *et al.* (2001). Citrin and aralar1 are Ca(2+)-stimulated aspartate/glutamate transporters in mitochondria. EMBO J 20, 5060–5069.
Palty R *et al.* (2010). NCLX is an essential component of mitochondrial Na+/Ca2 +exchange. Proc Natl Acad Sci USA 107, 436–441.
Pardo B, Contreras L, Serrano A, Ramos M, Kobayashi K, Iijima M, Saheki T, Satrustegui J (2006). Essential role of aralar in the transduction of small Ca2+ signals to neuronal mitochondria. J Biol Chem 281, 1039–1047.
Perocchi F, Gohil VM, Girgis HS, Bao XR, McCombs JE, Palmer AE, Mootha VK (2010). MICU1 encodes a mitochondrial EF hand protein required for Ca(2+) uptake. Nature 467, 291–296.
Plovanich M *et al.* (2013). MICU2, a paralog of MICU1, resides within the mitochondrial uniporter complex to regulate calcium handling. PLoS One 8, e55785.
Quintana A, Schwindling C, Wenning AS, Becherer U, Rettig J, Schwarz EC, Hoth M (2007). T cell activation requires mitochondrial translocation to the immunological synapse. Proc Natl Acad Sci USA 104, 14418–14423.
Raffaello A, De Stefani D, Sabbadin D, Teardo E, Merli G, Picard A, Checchetto V, Moro S, Szabo I, Rizzuto R (2013). The mitochondrial calcium uniporter is a multimer that can include a dominant-negative pore-forming subunit. EMBO J 32, 2362–2376.
Rizzuto R, De Stefani D, Raffaello A, Mammucari C (2012). Mitochondria as sensors and regulators of calcium signalling. Nat Rev Mol Cell Biol 13, 566–578.
Rizzuto R, Duchen MR, Pozzan T (2004). Flirting in little space: the ER/mitochondria Ca2+ liaison. Sci STKE 2004, re1.
Rizzuto R, Pinton P, Carrington W, Fay FS, Fogarty KE, Lifshitz LM, Tuft RA, Pozzan T (1998). Close contacts with the endoplasmic reticulum as determinants of mitochondrial Ca2 +responses. Science 280, 1763–1766.
Robinson KM, Janes MS, Pehar M, Monette JS, Ross MF, Hagen TM, Murphy MP, Beckman JS (2006). Selective fluorescent imaging of superoxide in vivo using ethidium-based probes. Proc Natl Acad Sci USA 103, 15038–15043.
Roy SS, Madesh M, Davies E, Antonsson B, Danial N, Hajnoczky G (2009). Bad targets the permeability transition pore independent of Bax or Bak to switch between Ca2+-dependent cell survival and death. Mol Cell 33, 377–388.
Salvioli S, Ardizzoni A, Franceschi C, Cossarizza A (1997). JC-1, but not DiOC6(3) or rhodamine 123, is a reliable fluorescent probe to assess delta psi changes in intact cells: implications for studies on mitochondrial functionality during apoptosis. FEBS Lett 411, 77–82.
Sancak Y *et al.* (2013). EMRE is an essential component of the mitochondrial calcium uniporter complex. Science 342, 1379–1382.
Satrustegui J, Contreras L, Ramos M, Marmol P, del Arco A, Saheki T, Pardo B (2007a). Role of aralar, the mitochondrial transporter of aspartate-glutamate, in brain N-acetylaspartate formation and Ca(2+) signaling in neuronal mitochondria. J Neurosci Res 85, 3359–3366.
Satrustegui J, Pardo B, Del Arco A (2007b). Mitochondrial transporters as novel targets for intracellular calcium signaling. Physiol Rev 87, 29–67.
Tewari SG, Dash RK, Beard DA, Bazil JN (2012). A biophysical model of the mitochondrial ATP-Mg/P(i) carrier. Biophys J 103, 1616–1625.
Thapa RJ, Basagoudanavar SH, Nogusa S, Irrinki K, Mallilankaraman K, Slifker MJ, Beg AA, Madesh M, Balachandran S (2011). NF-kappaB protects cells from gamma interferon-induced RIP1-dependent necroptosis. Mol Cell Biol 31, 2934–2946.
Traba J, Del Arco A, Duchen MR, Szabadkai G, Satrustegui J (2012). SCaMC-1 promotes cancer cell survival by desensitizing mitochondrial permeability transition via ATP/ADP-mediated matrix Ca(2+) buffering. Cell Death Differ 19, 650–660.
Trenker M, Malli R, Fertschai I, Levak-Frank S, Graier WF (2007). Uncoupling proteins 2 and 3 are fundamental for mitochondrial Ca2+ uniport. Nat Cell Biol 9, 445–452.
Uribe S, Rangel P, Pardo JP (1992). Interactions of calcium with yeast mitochondria. Cell Calcium 13, 211–217.
Wei AC, Liu T, Cortassa S, Winslow RL, O'Rourke B (2011). Mitochondrial Ca2+ influx and efflux rates in guinea pig cardiac mitochondria: low and high affinity effects of cyclosporine A. Biochim Biophys Acta 1813, 1373–1381.
Wibom R *et al.* (2009). AGC1 deficiency associated with global cerebral hypomyelination. N Engl J Med 361, 489–495.
Zhou Z, Matlib MA, Bers DM (1998). Cytosolic and mitochondrial Ca2+ signals in patch clamped mammalian ventricular myocytes. J Physiol 507, 379–403.
Zoccarato F, Nicholls D (1982). The role of phosphate in the regulation of the independent calcium-efflux pathway of liver mitochondria. Eur J Biochem/FEBS 127, 333–338.